Applied Ocean Research 93 (2019) 101947

Contents lists available at ScienceDirect

Applied Ocean Research

journal homepage: www.elsevier.com/locate/apor

Probabilistic analysis of offshore wind turbines under extreme resonant response: Application of environmental contour method

Joey Velarde[*,a,b], Erik Vanem[c], Claus Kramhøft[a], John Dalsgaard Sørensen[b]

[a] Marine and Foundation Engineering, COWI A/S, Aarhus 8000, Denmark
[b] Department of Civil Engineering, Aalborg University, Aalborg 9220, Denmark
[c] DNV GL Group Technology and Research, Høvik 1322, Norway

ARTICLE INFO

Keywords:
Environmental contour method
Probabilistic design
Reliability analysis
Dynamic response
Offshore wind turbines
Marine structures

ABSTRACT

Offshore wind turbines can exhibit dynamic resonant behavior due to sea states with wave excitation frequencies coinciding with the structural eigenfrequencies. In addition to significant contributions to fatigue actions, dynamic load amplification can govern extreme wind turbine responses. However, current design requirements lack specifications for assessment of resonant loads, particularly during parked or idling conditions where aerodynamic damping contributions are significantly reduced. This study demonstrates a probabilistic approach for assessment of offshore wind turbines under extreme resonant responses during parked situations. Based on in-situ metocean observations on the North Sea, the environmental contour method is used to establish relevant design conditions. A case study on a feasible large monopile design showed that resonant loads can govern the design loads. The presented framework can be applied to assess the reliability of wave-sensitive offshore wind turbine structures for a given site-specific metocean conditions and support structure design.

1. Introduction

Current design practice for offshore wind turbine support structures are based on design codes, where appropriate safety levels have to be fulfilled for a number of design situations. These include, among others, designing against extreme wind and wave conditions, fault occurrence, and emergency shutdown cases. In spite of the extensive list, current design requirements lack specifications for assessment of structural resonance, where dynamic amplification can significantly increase extreme loads. This study investigates the design specifications related to structural resonance, particularly for hydrodynamically sensitive, bottom-fixed OWT structures.

Offshore wind turbines can exhibit resonant behavior due to sea states with wave period close to the natural frequency. In addition to significant contributions to fatigue actions, dynamic load amplification can govern extreme responses. Hence, this phenomenon can be considered as a critical event along with environmental conditions that correspond to severe wave height or extreme wind speed. The problem can be treated as a rare event, since the probability of having significantly large wave heights with wave period close to the first natural period of the structure is limited by the physical wave breaking phenomena. Although the maximum wave height before wave breaking can be predicted as a function of wave steepness, this breaking limit is not absolute and can always be influenced by site-specific physical and environmental characteristics. A well-established method for extrapolation of metocean parameters is the *environmental contour* (EC) method, which was first demonstrated by Haver [1–3] in defining design curves for extreme wave height and wave period in the Northern North Sea.

Responses of offshore structures cannot be predicted using a single metocean parameter, but rather by at least a joint distribution of wave height and wave period. Joint modeling of extreme wave heights (H_s) and corresponding conditional wave periods ($T_p|H_s$) have been demonstrated in several literature [2,4–7] based on Conditional Modeling Approach (CMA), which is widely applied in modeling multivariate extremes. The approach is efficient since the joint probabilistic information can be directly obtained from metocean data, either from direct measurements or hindcast predictions. Description of other approaches for joint metocean modeling can be found in several literature [8–11]. A detailed discussion of statistical modeling of environmental conditions can be found in the review by Jonathan and Ewans [12], which also highlights that there is currently no clear consensus in multivariate modeling within the metocean community.

Today's standard approach for constructing environmental contours is based on Inverse First Order Reliability Method (IFORM) introduced by Winterstein et al. [13], where the standard normal space is used to determine design variables for the given multivariate distributions and

* Corresponding author.
E-mail address: jovl@cowi.com (J. Velarde).

https://doi.org/10.1016/j.apor.2019.101947
Received 23 May 2019; Received in revised form 20 August 2019; Accepted 26 September 2019

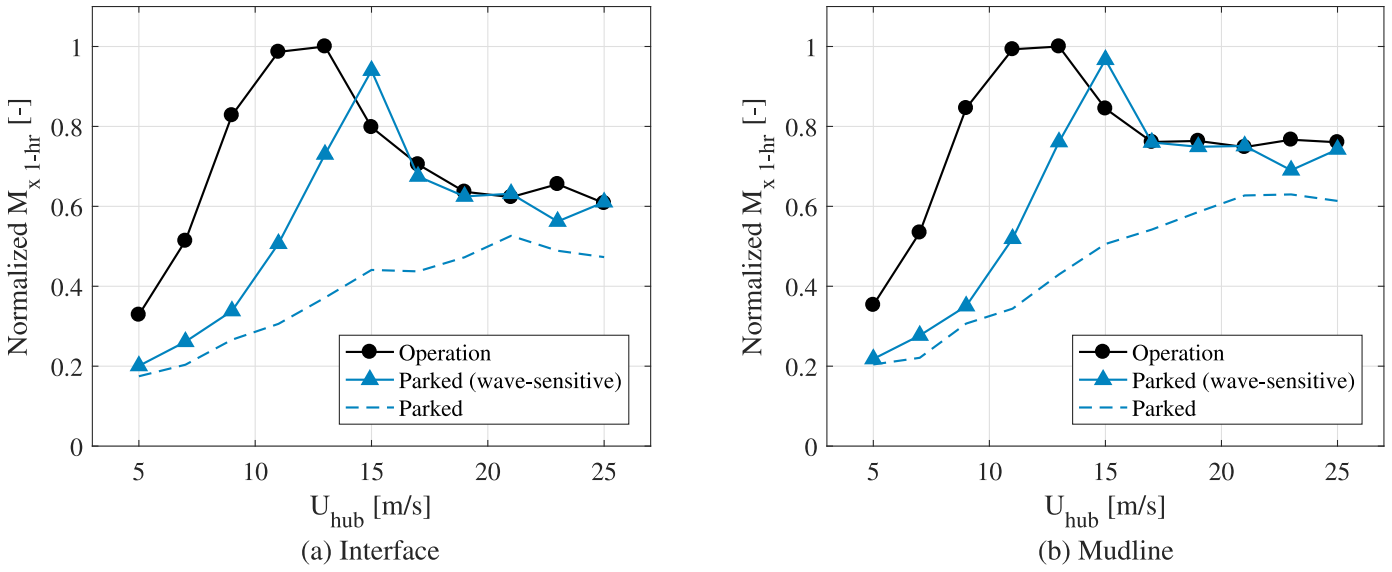

Fig. 1. Comparison of normalized most probable maximum bending moment ($M_{x\ 1-hr}$) at the (a) interface and (b) mudline during operation and parked conditions. Loads are derived from simulations under normal turbulence model (0.90 fractile) for a North Sea site at 25 m water depth.

specified return periods. An alternative to this traditional approach based on direct Monte Carlo simulations was proposed by Huseby et al. [14,15]. Since the contours are independent of the structural design, the EC method is an ideal alternative to full long-term response analysis (FLTA) when design loads are of main interest.

A number of literature demonstrate application of EC method for offshore structures. Christensen and Arnbjerg-Nielsen [16] applied the EC method to established OWT design loads and response distribution. The study also demonstrated calibration of partial safety factors for both extreme and operating conditions. Saranyasoontorn and Manuel [17] investigated the accuracy of EC method for derivation of OWT design loads. The study highlighted the importance of assessing both operation and parked cases to determine the governing design load. Agarwal and Manuel [18] applied the EC method to derive long-term OWT extreme loads. Results from peak-over-threshold (POT) approach and block maxima approach have shown good agreement for load distributions with well-defined tails. Baarholm et al. [19] investigated ringing phenomenon for the *Troll A Platform*, an offshore natural gas platform with concrete gravity based foundation installed in the Northern North Sea. Environmental contours were combined with platform response from model testing in order to verify the design loads. A modified EC method was introduced by Li et al. [20] to predict long-term extreme responses of bottom-fixed OWTs. The proposed method accounts for the non-monotoic OWT response, and therefore can substitute the traditional EC method in load cases where wind loads are significant. On a comparative study of different EC methods, Vanem [21] demonstrated that responses of a hypothetical one degree-of-freedom system can be governed by sea states with wave period close to the structural natural frequency. For offshore wind turbines (OWT), this resonant behavior is more critical and can lead to significant responses during parked conditions, as investigated by Shirdazeh et al. [22].

The aim of this paper is twofold. Firstly, it attempts to establish design conditions based on the EC method. Secondly, it demonstrates a probabilistic framework for assessment of extreme responses of wave-sensitive OWT structures under extreme resonant behavior during parked conditions. The identified uncertainty in design of large monopiles is further discussed in Section 2. The general methodology is summarized in Section 3, where the EC method, wind turbine modeling and reliability analysis are also discussed. The proposed probabilistic framework is demonstrated on a large monopile case study presented in Section 4. The last section presents the conclusions and recommendations. This study addresses the uncertainties related to specification of design conditions, particularly the need for a resonance ultimate limit state for larger bottom-fixed support structures.

2. Identified design uncertainty

The most accurate approach for deriving the long-term extreme response distribution of an OWT is by performing a full long-term analysis (FLTA), which is also referred to as the *all sea states approach*. This approach considers all site-specific environmental conditions, with a main disadvantage of being computationally expensive. For the 1-hour extreme response, X_{1-hr}, the long-term cumulative distribution function (CDF), $F_{X_{1-hr}}(x)$, can be expressed as shown in Eq. (1).

$$F_{X_{1-hr}}(x) = \int_u \int_h \int_t F'_{X_{1-hr}|U_w,H_s,T_p}(x|u,\ h,\ t) f_{U_w,H_s,T_p}(u,\ h,\ t)\, du\, dh\, dt \tag{1}$$

where $f_{U_w,H_s,T_p}(u,\ h,\ t)$ is the joint probability distribution function (PDF) of mean wind speed (U_w), significant wave height (H_s) and wave spectral period (T_p), and $F'_{X_{1-hr}|u,h,t}(x|u,\ h,\ t)$ is the short-term CDF of X_{1-hr} conditional on environmental parameters (U_w, H_s, T_p). Both terms represent the inherent randomness associated with the joint environmental PDF and short-term extreme responses, respectively.

For wave-dominated offshore structures where the main interest is the extreme responses due to extreme environmental conditions, the EC method or *contour line method* is commonly used as an alternative to FLTA. As an example, the 50-year extreme response can be estimated as the maximum response considering all the wind and wave conditions along the 50-year joint environmental contour. The variability in the short-term extreme response is then accounted for by taking the 0.85 to 0.95 fractile [23,24]. This approach, however, is not directly applicable to OWTs as demonstrated in several studies [17,18,20]. A discontinuous or non-monotonic response is observed for OWTs, since there is transition from operating state to parked state around cut-out wind speed (normally at 25 m/s). Thus, depending on site-specific conditions and wind turbine rating, the maximum load can be governed by the non-extreme operating wind conditions, particularly around rated or cut-out wind speeds.

Based on an extensive set of fatigue simulations for a large monopile supporting a 10 MW OWT [25], the most probable 1-hour short-term extreme bending moment ($M_{x\ 1-hr}$) during operation and parked situations are estimated as shown in Fig. 1. The values do not reflect short-

term variability and are normalized to ease comparison. For both interface and mudline, the maximum $M_{x\ 1-hr}$ is governed by the operation case. However, it is observed that a parked, wave-sensitive OWT can also give the same response magnitude as the operating case. These extreme loads are not caused by extreme H_s, but rather by moderate wave conditions with T_p close to the natural frequency. Disregarding the T_p distribution (i.e., by taking the most probable T_p for a given U_w, H_s combination as represented by the dashed line in Fig. 1) can underestimate responses during parked conditions. Note that in the case study considered, the extreme loads corresponding to the 50-year U_w and 50-year H_s have relative load magnitudes equal to 0.67 and 0.83 at the interface and mudline levels, respectively, and therefore do not govern the design.

It can be argued that the parked and operational loads presented above are not directly comparable, since assuming a 0.90 turbulence fractile does not give the same safety margins for both design situations. Loads during parked suituations are primarily governed by waves and are subject to higher uncertainties related to OWT dynamic response.

A schematic illustration of environmental contour and critical limit state functions in *U-space* is shown in Fig. 2. The limit state functions representing failure during operation ($g_1(z)$) and extreme environmental conditions ($g_2(z)$) are illustrated in Fig. 2a [17]. In addition, the limit state function for failure during parked situations under extreme resonant responses ($g_3(z)$) in the $H_s - T_p$ *U-space* is illustrated in Fig. 2b. This load case can be associated with parked or idling situations resulting from electrical faults. In practice, a wind turbine availablity of 90% is currently recommended by DNVGL [26] for assessment of fatigue of OWT components. Situations during installation phase, where OWTs can idle up to several months before power production commences, are additional scenarios where the risk of failure cannot be disregarded.

Although OWT substructures are designed such that the overall natural frequency is far away from the wave peak frequency, waves with period close to the structural natural period can develop resonant behavior, and become critical particularly for the parked case with

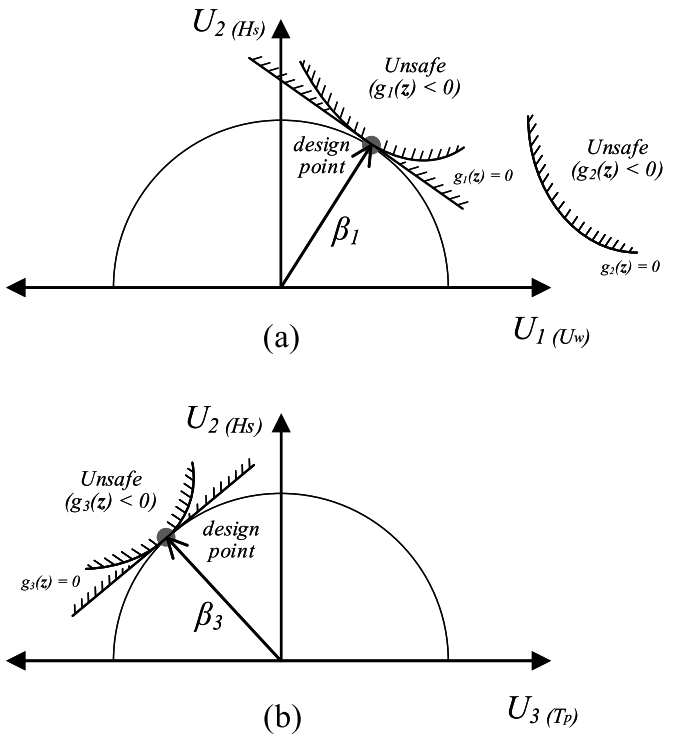

Fig. 2. Schematic 2D illustration of environmental contour, limit state functions and potential design points in (a) $U_w - H_s$ *U-space* and (b) $H_s - T_p$ *U-space* for wave-sensitive offshore wind turbines.

reduced aerodynamic damping. These extreme loads introduce design uncertainties for large, wave-sensitive monopiles, which are currently not covered by existing design standards. The succeeding sections address this problem based on the assumption that the extreme resonant loads govern the design.

3. Methods

The proposed framework for evaluation of OWT structural reliability is shown in Fig. 3. Based on in-situ metocean data, the environmental contours are constructed to define the relevant metocean conditions. An integrated OWT model is developed to carry out time-domain load simulations. Using the derived extreme load distribution, reliability assessment is performed for a selected limit state. The framework is demonstrated on a case study of a large monopile supporting a 10 MW OWT.

3.1. Environmental contour method

The EC method is a well-established approach for defining statistical descriptions of the metocean environment. Based on the first-order reliability method (FORM) [27], the inverse-FORM (IFORM) [13] is an efficient method to approximate a limit state surface for a given probability of failure (P_F) or target return period (T_R). Transformation of independent standard normal random variables (U_1, U_2) from the standard normal random space (U-space) to the physical parameters (H_s, T_p) in the physical space (X-space) is normally performed by Rosenblatt transformation [28].

Given a set of metocean data, the aim is to model the tail distribution and extrapolate at higher return values. Similar to Extreme Value analysis, return periods of interest are much longer than available measurements. Therefore, the uncertainty in defining a design sea state increases for higher return periods. As a practical rule of thumb, extrapolations to higher return periods are only reasonable up to about four times the length of the data [29] (e.g. for a given 20 years of continuous data, it is statistically sound to predict up to the 80-year return value).

Statistical extrapolation of metocean parameters using IFORM is widely accepted in several design standards, including DNV GL's *Environmental conditions and environmental loads (DNVGL-RP-C205)* [30], NORSOK's standard on *Actions and action effects (N-003)* [24] and IEC's *Design requirements for offshore wind turbines (IEC 61400-3)* [31]. The latter particularly describes a procedure for determining the 50-year significant wave height (H_s) conditional on mean wind speed (U_w) for ULS analysis during wind turbine power production.

3.1.1. Metocean data

In terms of data usage, EC method can be classified into two [6]: (1) the initial distribution or global approach, where all long-term data are used included in the analysis, and (2) the event approach, where only data exceeding a certain threshold are used in the analysis. Furthermore, site-specific metocean database should include long-term joint distribution of H_s, T_p or T_z, mean wave direction ($\bar{\theta}$), and wave directional spreading around the mean. However, these four parameters are not always available, so wave scatter diagrams are usually reduced to two or three parameters [29].

In this study, the initial distribution approach is performed in constructing $H_s - T_p$ contours. Different methods for constructing environmental contours are demonstrated using in-situ observations in four selected offshore sites as shown in Fig. 4. In-situ data representing 1-hour sea states are made available by the EU Copernicus Project and are described in Table 1. All succeeding illustrations of joint metocean modeling are derived based on Site 1 data from the Belgian North Sea.

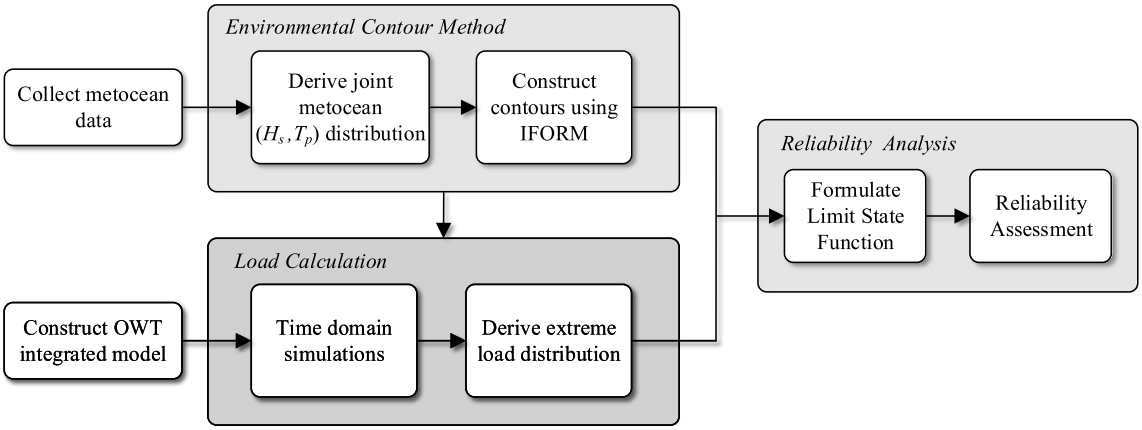

Fig. 3. General framework for evaluation of OWT structural reliability.

3.1.2. Joint metocean modeling

The long-term description of environmental conditions was estimated by fitting statistical joint distributions to the available wave data. A common practice is to fit a marginal distribution to H_s, and a conditional distribution to T_p. This model, which is referred to as ``H_s *marg.*'' in this paper, generally gives good approximations to extreme wave heights and corresponding wave periods, but can overestimate H_s at lower values of T_p due to physical limitations induced by wave steepness. When the main interest is the prediction of extreme values of H_s conditional on T_p close to the structural natural period (f_n), fitting a marginal distribution $f_{T_p}(t_p)$ to T_p and a conditional distribution $f_{H_s|T_p}(h, t_p)$ to H_s can avoid overestimation of H_s. This model, referred to as "T_p *marg.*" model, is also based on the initial distribution approach which could introduce bias in parameter estimation. An alternative model where $f_{H_s|T_p}(h|t_p)$ is fitted to the "tail" of the H_s distribution is also investigated and is referred to as the ``T_p *marg. (tail)*'' model. A description and comparison of these models are presented for the selected offshore sites.

H_s marg.model

When fitting the marginal distribution to H_s, the joint description ($f_{H_s,T_p}(h, t_p)$) of H_s and T_p can be formulated as follows:

Table 1
Data description for the four selected offshore sites.

Site No.	Country[a]	LAT (deg)	LONG (deg)	Data Coverage	
				Start	End
1	BE	51.41	2.77	01-01-2011	31-03-2018
2	NL	52.93	4.15	19-05-2011	31-12-2017
3	NL	54.12	4.02	01-01-2011	31-03-2018
4	NL	54.85	4.73	01-01-2014	31-03-2018

[a] BE: Belgium; NL: The Netherlands

$$f_{H_s,T_p}(h, t_p) = f_{H_s}(h) f_{T_p|H_s}(t_p|h) \tag{2}$$

The marginal distribution $f_{H_s}(h)$ is generally well approximated by a 3-parameter Weibull distribution with probability density function defined by Eq. (3). The Weibull shape (α_1), scale (β_1) and location (γ_1) parameters are the maximum likelihood estimates.

$$f_{H_s}(h) = \frac{\beta_1}{\alpha_1}\left(\frac{h-\gamma_1}{\alpha_1}\right)^{\beta_1-1} \exp\left[-\left(\frac{h-\gamma_1}{\alpha_{t_p}}\right)^{\beta_1}\right] \tag{3}$$

The conditional distribution $f_{T_p|H_s}(t_p|h)$ is modelled by fitting a

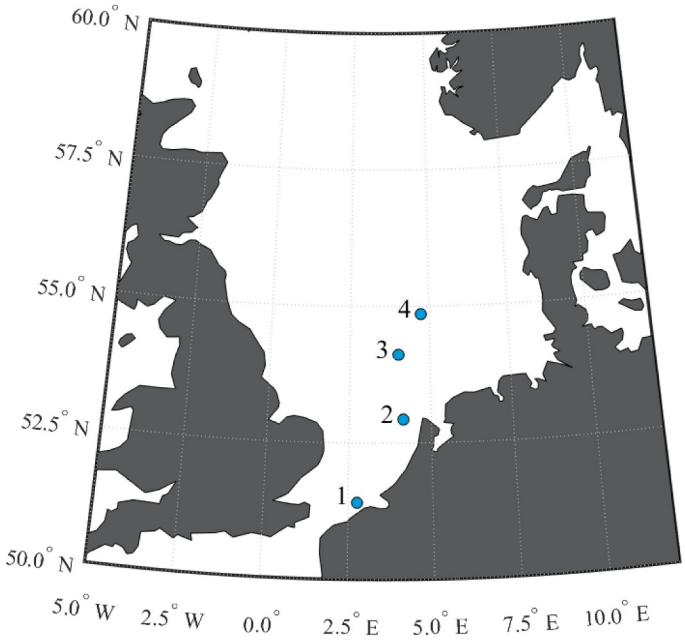

Fig. 4. Location of four in-site marine observation sites in the North Sea.

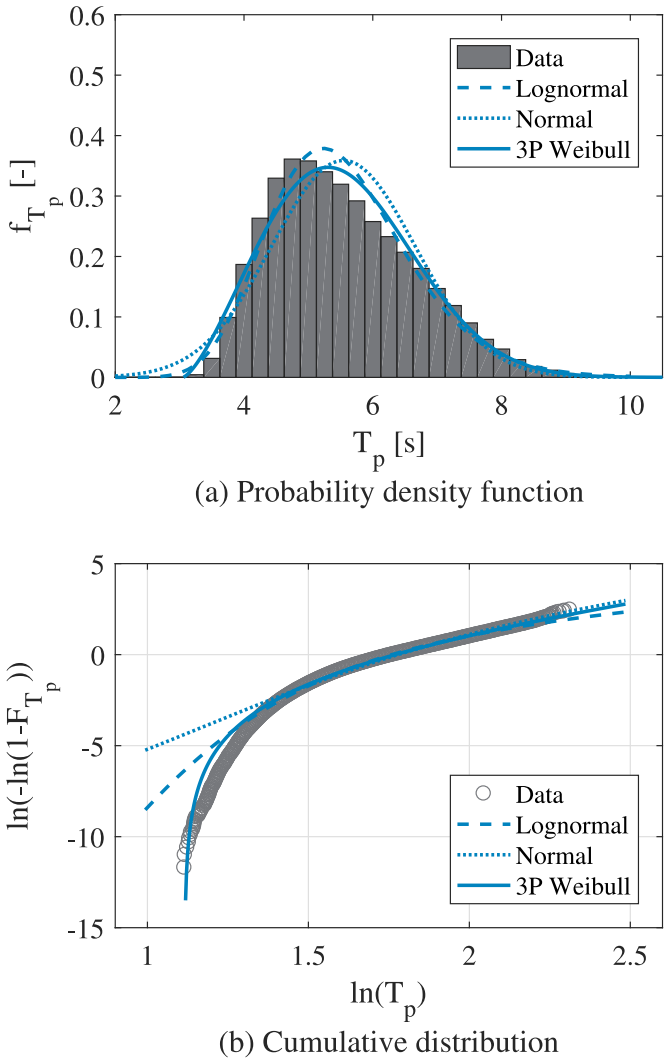

Fig. 5. Marginal T_p distribution for 1-hour sea states at Site 1: (a) probability density function ($f_{T_p}(t)$); (b) cumulative distribution function ($F_{T_p}(t)$).

lognormal distribution with probability density function defined by Eq. (4). The lognormal mean (μ_1) and standard deviation (σ_1) are conditional on the wave height (h) based on nonlinear functions defined by Eqs. (5) and (6), respectively. The derived parameters are summarized in Appendix Table A1.

$$f_{T_p|H_s}(t_p|h) = \frac{1}{t_p\sigma_1\sqrt{2\pi}}\exp\left[\frac{-(\ln(t_p)-\mu_1)^2}{2\sigma_1^2}\right] \quad (4)$$

$$\mu_{LN} = a_1 + a_2 h^{a_3} \quad (5)$$

$$\sigma_{LN} = b_1 + b_2\exp(b_3\, h) \quad (6)$$

T_p marg.model

When fitting the marginal distribution to T_p, the joint description ($f_{T_p,H_s}(t_p, h)$) can be formulated as follows:

$$f_{T_p,H_s}(t_p, h) = f_{T_p}(t_p) f_{H_s|T_p}(h|t_p) \quad (7)$$

Similarly, the marginal distribution $f_{T_p}(t_p)$ is generally well approximated by a 3-parameter Weibull distribution as illustrated in Fig. 5. The probability density function is defined by Eq. (8), where α_2, β_2 and γ_2 are the maximum likelihood estimates of the shape, scale and location parameters, respectively.

$$f_{T_p}(t_p) = \frac{\beta_2}{\alpha_2}\left(\frac{t_p-\gamma_2}{\alpha_2}\right)^{\beta_2-1}\exp\left[-\left(\frac{t_p-\gamma_2}{\alpha_2}\right)^{\beta_2}\right] \quad (8)$$

The conditional distribution $f_{H_s|T_p}(h|t_p)$ is modelled by fitting a 2-parameter Weibull distribution with probability density function defined by Eq. (3). The shape ($\alpha_3(t_p)$) and scale ($\beta_3(t_p)$) parameters are calculated conditional on t_p based on the nonlinear functions defined by Eqs. (10) and (11). The derived parameters are summarized in Appendix Table A2.

$$f_{H_s|T_p}(h|t_p) = \frac{\beta_3}{\alpha_3}\left(\frac{h}{\alpha_3}\right)^{\beta_3-1}\exp\left[-\left(\frac{h}{\alpha_3}\right)^{\beta_3}\right] \quad (9)$$

$$\alpha_3 = m_1 + m_2 t_p^{m_3} \quad (10)$$

$$\beta_3 = n_1 + n_2 t_p^{n_3} \quad (11)$$

T_p marg. (tail) *model*

To improve approximation of the tail behavior, an alternative approach where the conditional distribution $f_{H_s|T_p}(h|t_p)$ is fitted to the upper tail of H_s distribution (i.e. H_s above the 95% quantile) by the least squares (LS) method. The fitting method is illustrated in Appendix Fig. B1, Fig. B2 and Fig. B3 for lower T_p bins, while Fig. B4 illustrates the fitting for a higher T_p bin.

For lower T_p bins, fitting to the distribution tail does not significantly improve the fit, due to errors in nonlinear fitting of the derived parameters across the T_p range. For higher T_p bins where directionality effects can introduce bi- or multimodal distributions, fitting to the tail of the distribution can avoid the bias and lead to tighter environmental contours. The T_p *marg.* (*tail*) model adopts the same marginal distribution (Eq. (8)), with modified conditional distribution described by the Eqs. (12)–(14). The derived parameters are summarized in Appendix Table A2.

$$f_{H_s|T_p}(h|t_p) = \frac{\beta_4}{\alpha_4}\left(\frac{h}{\alpha_4}\right)^{\beta_4-1}\exp\left[-\left(\frac{h}{\alpha_4}\right)^{\beta_4}\right] \quad (12)$$

$$\alpha_4 = p_1 + p_2 t_p^{p_3} \quad (13)$$

$$\beta_4 = q_1 + q_2 t_p^{q_3} \quad (14)$$

The advantage of the H_s *marg.* model is that the conditional standard deviation $\sigma_1(t_p|h)$ approaches zero for increasing h, as illustrated in Fig. 6. On the other hand, the conditional standard deviation of the T_p *marg.* model $\sigma_{WBL}(t_p|h)$, derived from Weibull parameters $\alpha_3(h|t_p)$ and $\beta_3(h|t_p)$, increases with t_p. This inflates the contours

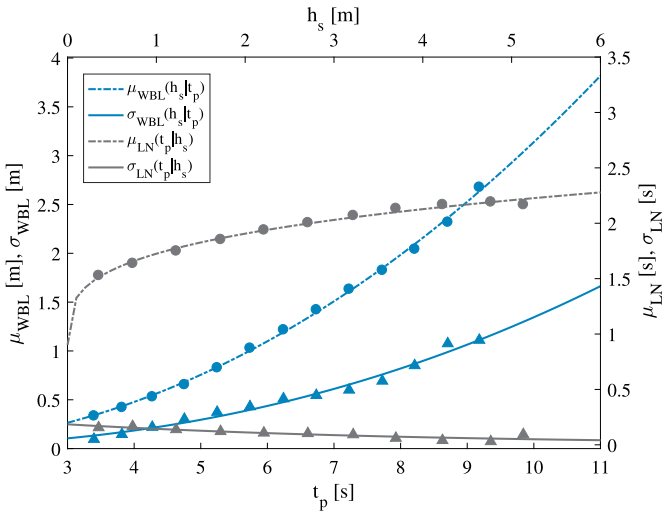

Fig. 6. Nonlinear estimates of conditional Weibull (μ_{WBL}, σ_{WBL}) and lognormal (μ_{LN}, σ_{LN}) distribution parameters derived for Site 1 data.

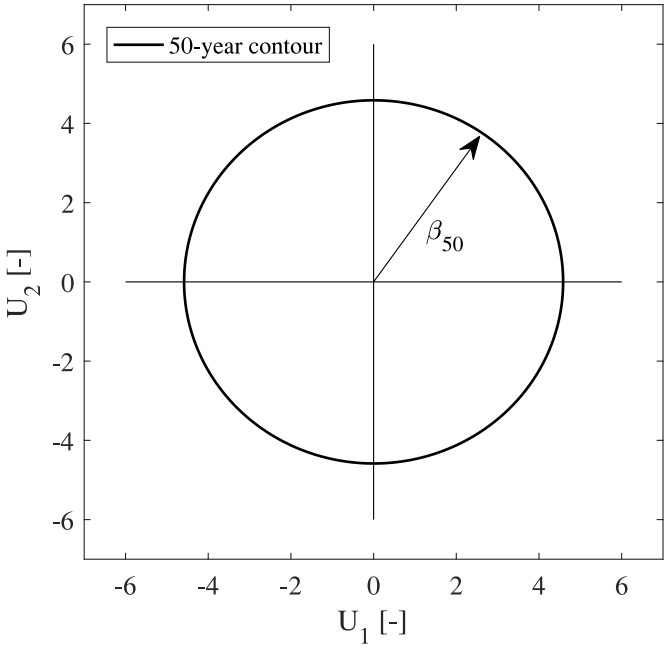

Fig. 7. U-space representation given $\beta_{50} = 4.58$.

when extrapolating to higher t_p values, thus overestimating the extreme H_s values. The consequences of choosing either of the models presented are discussed in the succeeding section.

3.1.3. Environmental contours based on IFORM

For a specified return period (T_R) or probability of failure (P_F), the reliability index (β) can be determined based on the relation $\beta = -\Phi^{-1}(P_F)$. The corresponding isoline with radius equal to β can be constructed in the standard Gaussian space as a function of the independent standard Normal random variables (U_1, U_2), which satisfy Eq. (15) as illustrated in Fig. 7. Based on data representing 1-hour stationary sea states, the P_F for the 50-year U_1 or U_2 can be estimated as $P_{F50} = 1/(365*24*50) \approx 2.28 \cdot 10^{-6}$. Consequently, $\beta_{50} = 4.58$.

$$U_1^2 + U_2^2 = \beta^2 \tag{15}$$

The environmental contours are derived by mapping U_1 and U_2 into the physical space (T_p, H_s). By using Rosenblatt transformations [28], the cumulative distribution functions can be expressed in terms of the standard Normal distribution function (Φ) as defined by Eqs. (16) and (17). For the T_p *marg.* model, the Weibull cumulative distribution functions for both marginal $F_{T_p}(t_p)$ and the conditional $F_{H_s|T_p}(h_s|t_p)$ distributions are defined by Eqs. (18) and (19), respectively.

$$\Phi(U_1) = F_{T_p}(t_p) \tag{16}$$

$$\Phi(U_2) = F_{H_s|T_p}(h_s|t_p) \tag{17}$$

$$F_{T_p}(t_p) = 1 - \exp\left[-\left(\frac{t_p - \gamma_2}{\alpha_2}\right)^{\beta_2}\right] \tag{18}$$

$$F_{H_s|T_p}(h|t_p) = 1 - \exp\left[-\left(\frac{h}{\alpha_3}\right)^{\beta_3}\right] \tag{19}$$

To assess the validity of extrapolated wave heights, the generated contours are compared against limiting steepness values. The average wave steepness (S_p) for short-term irregular sea states is defined by Eq. (20) [30]. In cases where no reliable information is available, the limiting values for S_p can be approximated by Eq. (21), interpolated linearly for $8 < T_p < 15$ s. These limiting values were derived from measured data from the Norwegian Continental Shelf and are assumed to be generally valid. Based on the derive contours and in-situ data, the steepness criteria can be generally used in predicting the highest possible H_s. The defined criterion is not overconservative for lower T_p ranges up to 5 sec.

$$S_p = \frac{2\pi}{g}\frac{H_s}{T_p^2} \tag{20}$$

$$S_p = \begin{cases} 1/15, & \text{for } T_p \le 8 \text{ s.} \\ 1/25, & \text{for } T_p \ge 15 \text{ s.} \end{cases} \tag{21}$$

As discussed in several literature [12,32], a number of factors, both physical and statistical in nature, must be considered when extrapolating metocean conditions. Statistical considerations include the choice of distribution, the fitting method, length of data, and data quality related to instrumental errors and sampling variability. Physical factors, such as effect of directionality, wind seas and swells, and climate uncertainty, also contribute to the total uncertainty. These factors are not considered in this study.

3.2. Wind turbine modeling

3.2.1. Large monopile design

A preliminary monopile and tower design is established to support a 10 MW reference OWT [33]. Table 2 summarizes the wind turbine properties and foundation design parameters. Primary dimensions of the monopile are designed such that the natural frequency (f_n) of the OWT is outside the blade passing frequencies (1P and 3P). This is also normally within the *soft-stiff* region as illustrated in Fig. 8.

Based on a simplified fatigue reliability analysis, a 110 mm thickness is required at mudline for a design life of 25 years. This corresponds to a monopile D/t ratio = 73. The monopile thickness is varied from D/t = 73 at the mudline to D/t = 100 at the interface level. A tower with a total length of 96 m connects the interface to the hub height. The tower has a diameter of 6.5 m at the interface, and tapers gradually to 5.5 m at the top. In HAWC2 [34], the tower is modelled as 10 different sections with thickness ranging from 20 mm to 32 mm. The resulting OWT natural frequency is $f_n = 0.20$ Hz.

Note that wave excitation frequencies should practically be avoided in the design. Further increase in the target f_n would require a larger pile diameter up to 9.5 m, as demonstrated in several studies [35,36]. For a mean water depth of 25 m with a relatively mild wave climate, a pile diameter of 8.0 m is a feasible design.

3.2.2. Offshore wind turbine model

Wind turbine loads are calculated using HAWC2 [34], an aeroelastic simulation tool capable of both static and dynamic wind turbine analyses. HAWC2 is based on a multibody structural formulation, where each structural component is modelled by Timoshenko beam elements. The integrated model of an OWT supported by a monopile is illustrated in Fig. 9.

The OWT model is defined by structural elements with six degrees

Table 2
Wind turbine and monopile design parameters.

Parameter	Value
Rating [MW]	10
Rotor diameter [m]	178.3
Number of blades [−]	3
Cut-in, rated, cut-out U_w [m/s]	4.0, 11.4, 25.0
Rotor speed range [rpm]	6, 9.6
Hub height [m]	114
Interface elevation [m]	14.7
Mean water depth [m]	25
Monopile diameter [m]	8.0
Monopile thickness[a] [mm]	110

[a] Defined by ratio $D/t = 73$ at mudline

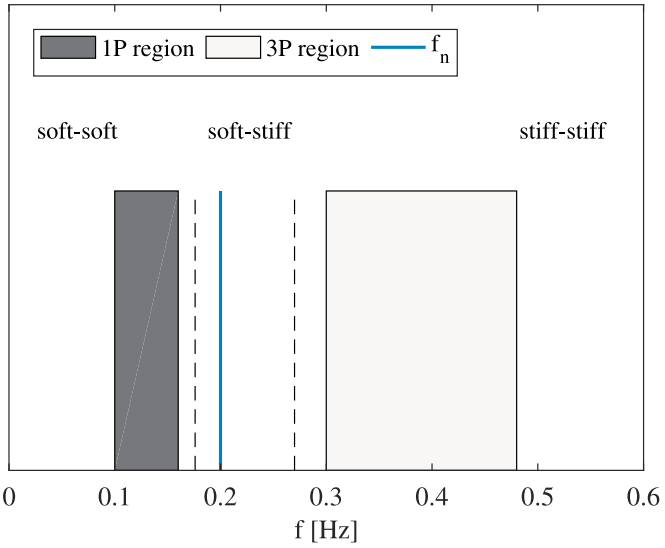

Fig. 8. DTU 10 MW reference wind turbine frequency ranges with 10% safety margin.

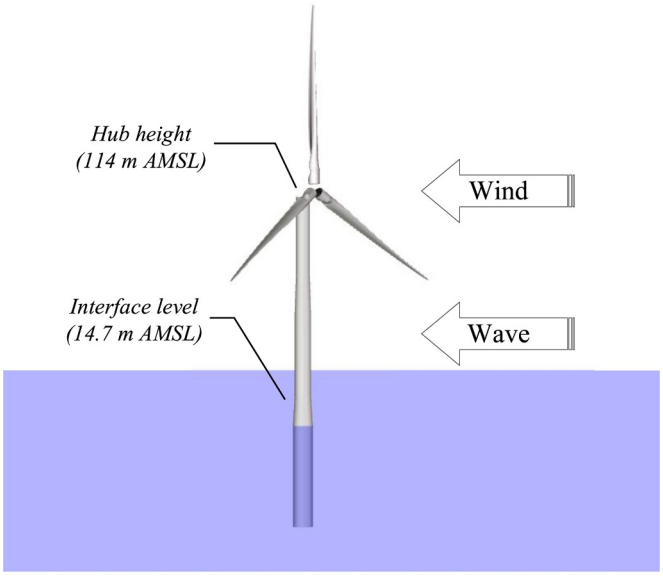

Fig. 9. Monopile model in HAWC2.

of freedom (x) and by matrices representing the mass [M], damping [D] and stiffness [K]. Considering both aerodynamic (F_{aero}) and hydrodynamic (F_{hydro}) forces, the general equation of motion can be expressed as shown in Eq. (22). The details of structural modeling and environmental loads calculation are further discussed in the following subsections.

$$[M]\ddot{x} + [D]\dot{x} + [K]x = F_{aero} + F_{hydro} \tag{22}$$

Structural model

The monopile, tower and rotor are all modelled as separate bodies. A linear elastic material is assumed for both monopile and steel tower, with Young's modulus, $E_s = 210$ GPa and shear modulus, $G_s = 80.8$ GPa. Both wind turbine nacelle and hub masses are represented as point masses at appropriate elevations. A simplified foundation model based on *apparent fixity* (AF) approach is implemented, where soil lateral and rotational stiffness are approximated by fixing the monopile at a certain distance below the mudline. A predetermined length of 24 m (3 times the pile diameter) is assumed.

The total damping (D_{total}) in an OWT can be modelled as the linear

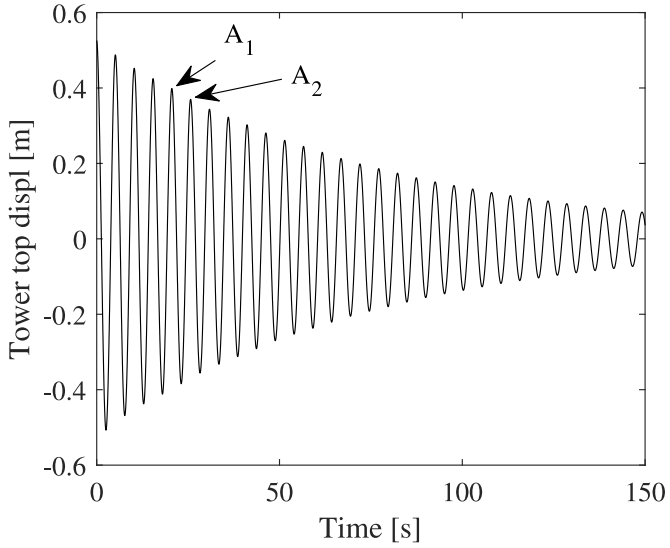

Fig. 10. Free vibration test with initial tower displacement of 0.50 m.

sum of foundation (D_{soil}), structural (D_{struc}), hydrodynamic (D_{hydro}) and aerodynamic (D_{aero}) damping as shown in Eq. (23). In HAWC2, structural damping is based on the classical Rayleigh viscous damping [37], where the total damping is calculated as a linear sum of mass and stiffness matrices. The damping coefficients were tuned such that the combined soil (D_{soil}) and structural damping (D_{struc}) leads to a damping ratio, $\zeta = 1.05\%$, for both first fore-aft and first side-to-side bending modes. A free vibration test, illustrated in Fig. 10, is performed to verify the damping ratio based on Eqs. (24) and (25). The damping level is a typical assumptions during design stage, and have been observed in several offshore measurement campaigns [22,38]. In addition, both aerodynamic and hydrodynamic damping are included in the simulations as a function of wind and wave parameters, respectively.

$$D_{total} = D_{soil} + D_{struc} + D_{hydro} + D_{aero} \tag{23}$$

$$\delta = \ln \frac{A_1}{A_2} \tag{24}$$

$$\zeta = \frac{\delta}{\sqrt{(2\pi)^2 + \delta^2}} \tag{25}$$

Environmental loads

The structural integrity of an OWT has to be verified against several design load cases (DLC), as outlined in design standards such as the IEC 61400-3 [31] and DNVGL-ST-0437 [26]. In this study, emphasis is made on DLC 6.4, where loads during idling case under operational wind conditions can govern the design. For hydrodynamically sensitive structures, such as large monopiles, the investigation is most critical for sea states with wave period close to the OWT's natural frequency.

Time-domain simulations are performed for 600 s at a timestep (Δt) of 0.02 s. The correlation between wind speed at hub height (U_w) and significant wave height (H_s) is based on wind farm data as illustrated in Fig. 11a. Wind speeds are generated assuming a power law profile with shear exponent, $\alpha = 0.15$. For every U_w, the turbulence intensity (TI) is defined by Eqs. (26) and (27) based on Normal Turbulence Model (NTM) [26,31] as illustrated in Fig. 11b. A reference value of $I_{ref} = 0.12$ was assumed for category C (low turbulence) and class III wind turbines. The wind fields generated in HAWC2 are based on Mann turbulence model [39]. Based on the wind profiles, aerodynamic drag loads for a parked turbine are calculated. The aerodynamic loads during wind turbine power production are based on the *blade element momentum (BEM)* theory [40,41].

$$\sigma_1 = I_{ref}(0.75V_{hub} + b); \quad b = 5.6\ m/s \tag{26}$$

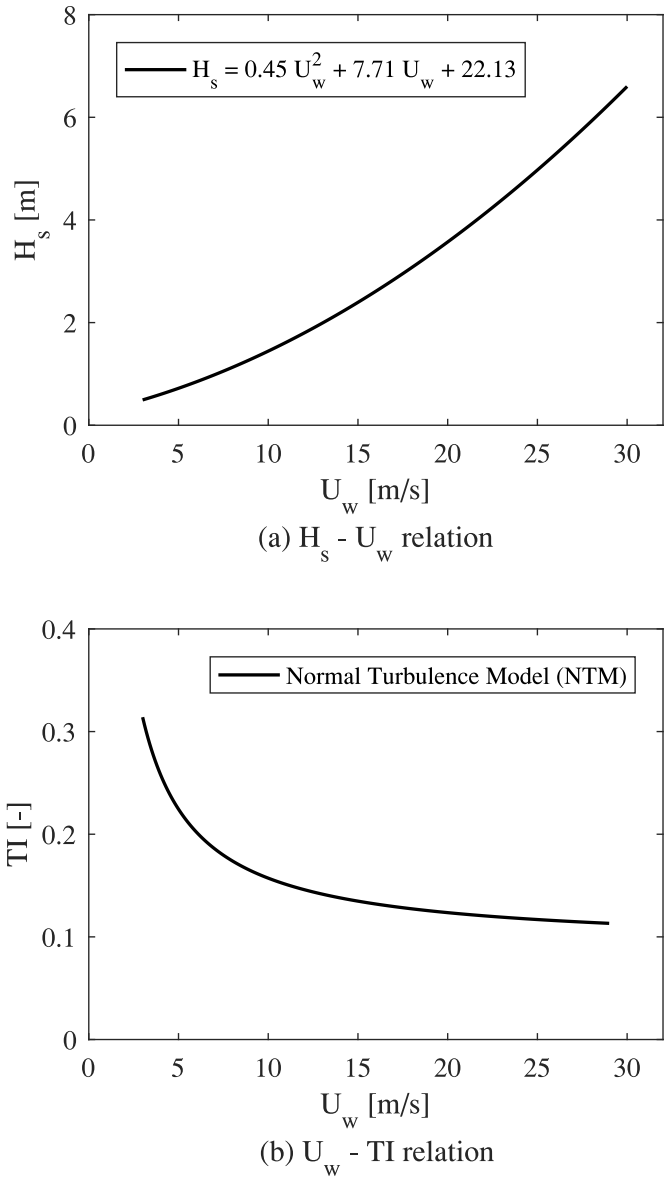

Fig. 11. (a) $H_s - U_w$ relation based on wind farm data; and (b) $U_w - TI$ relation based on Normal Turbulence Model (NTM).

$$TI = \sigma_1 / U_w \tag{27}$$

For each sea state, linear irregular waves were generated based on JONSWAP spectrum. The peak enhancement factor (γ) is defined by Eq. (28), where H_s and T_p are expressed in meters and in seconds, respectively [30].

$$\gamma = \begin{cases} 5, & \text{for } T_p/\sqrt{H_s} \leq 3.6. \\ \exp(5.75 - 1.15\frac{T_p}{\sqrt{H_s}}), & \text{for } 3.6 < T_p/\sqrt{H_s} < 5. \\ 1, & \text{for } 5 \leq T_p/\sqrt{H_s}. \end{cases} \tag{28}$$

Based on Morison's equation, the total hydrodynamic force per unit length of the monopile can be calculated as the sum of drag and inertia components as defined by Eq. (29). The load is applied at the instantaneous wave elevation. A drag coefficient, $C_D = 1.05$ and inertia coefficient, $C_M = 2.00$ are assumed.

$$F_{hydro} = \rho C_D D U|U| + \rho C_M A \dot{U} \tag{29}$$

3.2.3. Extreme load distribution

Before reliability analyses can be performed, an extreme load distribution has to be derived. The contours for specified return periods are shown in Fig. 12. The main interests are the extrapolated H_s, particularly at the region where resonant behavior is observed. Note that the resonant region depends on the structural design, and is independent of the environmental contours. The environmental contours, even for a return period of 1000 years, are found to be consistent with the steepness criteria [30]. In cases where limited metocean data is available, the defined criteria can be used to arrive at a conservative H_s for a given wave period. A summary of derived sea states for different annual probability of exceedance (q) is shown in Table 3.

For a wave dominated response, the long-term distribution can be approximated by Eq. (30). The variability in short-term structural response can be accounted for by inflating the environmental contours, as demonstrated by Winterstein et al. [13]. Alternatively, selecting a high fractile value for the extreme value distribution also results to a consistent load estimate. A 0.85 to 0.95 fractile value is recommended in literature [23] and in NORSOK standard for *Actions and action effects* [24].

Based on the sea states summarized in Table 3, OWT simulations with 1-hour basic time interval are performed in HAWC2. An extreme value distribution (Gumbel) given by Eq. (31) is fitted to the 0.90 fractile of the largest values obtained from 12 independent realizations, particularly at higher return periods 10, 50, 100 and 500 years. The derived annual load distribution is a main input to reliability assessment.

$$F_{M_x}(x) = \int_h \int_t F_{M_x|H_s,T_p}(x|h,\, t) f_{H_s,T_p}(h,\, t)\, dt\, dh \tag{30}$$

$$F_{M_x}(x) = \exp\left[-\exp\left(-\frac{x - \alpha_x}{\beta_x}\right)\right] \tag{31}$$

where α_x and β_x are the Gumbel location and scale parameters, respectively.

3.3. Reliability assessment

The reliability with respect to failure due to bending of tubular members is evaluated. Results from deterministic design equation is first presented for comparison with the calculated reliability indices.

3.3.1. Deterministic design check

For a deterministic, code-based design [42], the design equation for bending of tubular members is defined by Eq. (32).

$$M_{Sd} \leq M_{Rd} = \frac{f_{m,c} W}{\gamma_M} \tag{32}$$

where:

M_{Sd} is the design bending moment
M_{Rd} is the section design bending moment capacity
W is the elastic section modulus
γ_M is the material safety factor

The characteristic bending strength ($f_{m,c}$) is calculated as a function of characteristic yield strength ($f_{y,c}$), Young's modulus of elasticity ($E = 210\ GPa$), section outer diameter (d_o) and section thickness (t)

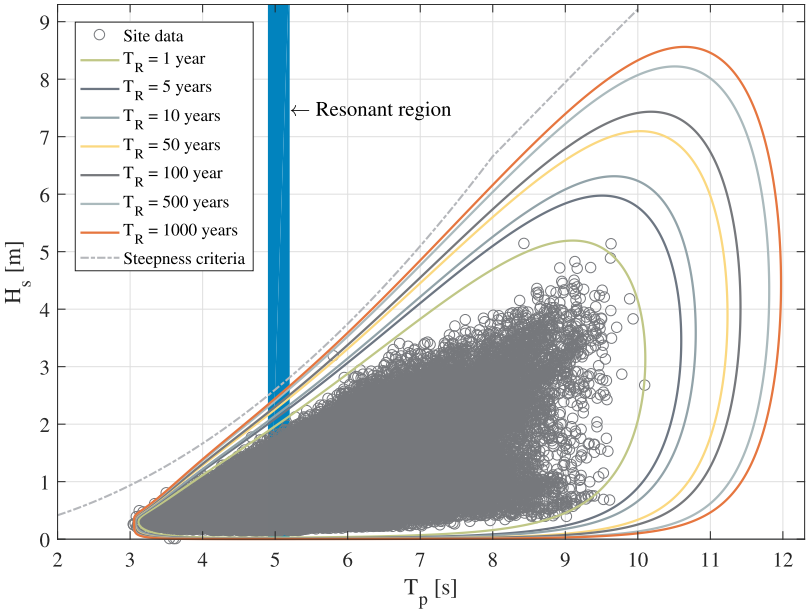

Fig. 12. Derived environmental contours based on the T_p *marg.* model and Site 1 data.

Table 3
Sea states for derivation of resonant response distribution.

q [-]	TR [yr]	Hs [m]	Tp [s]	Uw [m/s]
0.63	1	2.05	5.10	18.7
0.20	5	2.19	5.10	19.7
0.10	10	2.24	5.10	20.0
0.02	50	2.36	5.10	20.9
0.01	100	2.41	5.10	21.2
0.002	500	2.59	5.10	22.4
0.001	1000	2.63	5.10	22.7

as defined by Eq. (33). The equation is valid for $0.10 < \frac{f_y d_o}{Et} \leq 120\frac{f_y}{E}$.

$$f_{m,c} = \left[0.94 - 0.76\left(\frac{f_{y,c} d_o}{E_s t}\right)\right]\left(\frac{Z}{W}\right) f_{y,c} \tag{33}$$

where W and Z are the elastic section modulus and plastic section modulus, respectively, defined as follows:

$$W = \frac{\pi}{32}\frac{[d_o^4 - (d_o - 2t)^4]}{d_o} \tag{34}$$

$$Z = \frac{1}{6}[d_o^3 - (d_o - 2t)^3] \tag{35}$$

Using Eqs. (32) to (35), M_{Rd} can be estimated assuming $\gamma_M = 1.1$. A steel grade of *S*355 is assumed for both monopile and tower. A load safety factor, $\gamma_L = 1.35$, is applied to estimate M_{Sd} based on the most probable 50-year resonant load. For different section thickness (t), the ulitization ratio (M_{Sd}/M_{Rd}) is estimated as summarized in Table 4. Based on the calculated design values, the interface is more critical for failure due to dynamic resonant amplification.

The relatively high D/t ratio for large monopile and tower increases the slenderness ratio. The simplified design equation does not account for further reduction in strength due high D/t ratio. In addition, local, global, and shell buckling failure are not investigated in this example.

3.3.2. Limit state equation

Based on the design equations, a simplified limit state equation for bending of tubular members [42] can be formulated as defined by Eq. (36). The stochastic load is a function of the derived annual maximum bending moment (M_x) due to resonance phenomenon, with additional parameter X_{wave} to account for the wave load model uncertainty.

$$g(\mathbf{x}) = \left[0.94 - 0.76\left(\frac{f_y d_o X_{d_o}}{E_s t X_t}\right)\right]\frac{1}{6}[(d_o X_{d_o})^3 - (d_o X_{d_o} - 2tX_t)^3] f_y X_R - M_x X_{wave} \tag{36}$$

Table 4
Design bending moment resistance (M_{Rd}) and utilization ratios (M_{Sd}/M_{Rd}) for tower section at interface and monopile section at mudline.

Interface (tower)			Mudline (monopile)		
t_{twr} [mm]	M_{Rd} [MNm]	M_{Sd}/M_{Rd} [−]	t_{MP} [mm]	M_{Rd} [MNm]	M_{Sd}/M_{Rd} [−]
32	288.2	0.81	110	1583.8	0.22
30	263.7	0.89	100	1430.4	0.24
28	239.2	0.98	90	1276.3	0.27
26	214.6	1.09	80	1121.4	0.31

Table 5
Stochastic variables for bending of tubular members. G: Gumbel; LN: LogNormal; D: Deterministic.

Variable	Dist.	Interface		Mudline		Ref.
		Mean	COV	Mean	COV	
M_x [MNm]	G	165.9	0.016	237.4	0.027	[a]
f_y [MPa]	LN	414.0	0.05	354.0	0.05	-
E_s [GPa]	LN	210	0.03	210	0.03	[43]
X_{wave} [−]	LN	1.0	0.05-0.3	1.0	0.05-0.3	[43]
X_R [−]	LN	1.0	0.10	1.0	0.10	-
X_{d_o} [−]	LN	1.0	0.005	1.0	0.005	-
X_t [−]	LN	1.0	0.0025	1.0	0.0025	-
d_o [m]	D	6.5	-	8.0	-	[b]
t [mm]	D	26, 28, 30, 32	-	80, 90, 100, 110	-	[b]

[a] refer to Section 3.2.3
[b] refer to Section 3.2.1

Table 5 summarizes the load and resistance models' stochastic variables. The yield strength (f_y), which varies according to steel grade and section thickness, represents variability in material properties. The mean and COV for both monopile ($f_{y\,MP}$) and tower ($f_{y\,tower}$) yield strength are based on a steel grade of *S*355. The assumed mean and COV for the geometrical parameters (X_{d_o}, X_t) are considered representative for steel components. In addition, the assumed COV for X_{wave} are consistent with the recommendations from the *Probabilistic Model Code* [43], which states that the wave model uncertainty can vary from 0.05 to 0.30. For an assumed resistance model uncertainty (X_R), both monopile and tower designs are assessed at mudline and interface levels, respectively.

3.3.3. Reliability assessment

Failure is defined as the state where the yield strength is exceeded, which occurs if the limit state equation is less than or equal to zero. By definition, the probability of failure (P_F) and annual reliability index ($\beta(\mathbf{x})$) are given by Eqs. (37) and (38):

$$P_F(\mathbf{x}) = P_r(g(\mathbf{x}) \leq 0) \tag{37}$$

$$\beta(\mathbf{x}) \approx -\Phi^{-1}(P_F(\mathbf{x}) \cdot f_{park}) \tag{38}$$

where $\Phi()$ is the standardized normal distribution. Eq. (37) gives the conditional probability of failure given that the turbine is parked, stopped or idling during operational range of wind speeds. To account for this, Eq. (38) is modified to include the occurrence factor, f_{park}, here assumed to be 10%. Based on Eqs. (36)–(38), the reliability indices are estimated using FORM [27]. According to design codes [43,44], a target annual reliability index, $\beta = 3.3$ ($P_F \approx 5{\cdot}10^{-4}$) is recommended for ULS design of OWT. This corresponds to structures with relatively large cost of safety measures and minor consequences of failure.

4. Case study: large monopile

4.1. Environmental contours

A comparison of the 50-year $H_s - T_p$ contours based on the three EC models presented, namely the H_s *marg.*, T_p *marg.* and T_p *marg. tail*, is shown in Fig. 13. Although the H_s *marg.* model has an overall tighter contour at extreme H_s, T_p values, H_s prediction at lower T_p extends above the indicative steepness criteria for all offshore sites investigated. On the other hand, the T_p *marg.* model provides a better fit at T_p ranges of interest, at the expense of overestimating extreme H_s, T_p values. Lastly, the T_p *marg.* (*tail*) model gave an overall tighter fit for H_s across T_p values, but is prone to errors in generalizing the conditional parameters (Eqs. (13) and (14)) across T_p range. This can result to overestimating H_s at lower T_p ranges, as in the case of Sites 2 and 4. Note that the choice of statistical distributions are fitted for Site 1 data, which has a relatively mild sea state compared to the other offshore sites. The derived contours for the other offshore sites can be further refined by investigating other distribution types. This is not performed in this study.

The choice of model largely depends on the desired application. In this study, where interest is on the extrapolation of H_s at lower T_p ranges ($3 - 6\ s$), the T_p *marg.* model is preferred.

4.2. Wind turbine loads

To investigate the wave-induced resonant response, simulations based on DLC 6.4 were performed for different combinations of H_s and T_p. For demonstration of the resonance problem, only one realization is performed. The 10-minute maximum bending moment ($Mx_{\max}$) at the interface and mudline are used to derive the monopile response isolines. Fig. 14 shows the combined plot of the derived response isolines and environmental contours. The graphical solution shows peak responses around the structural natural period ($T_n = 5.1\ sec$), while the environmental contours show the occurrence probability of the sea states (H_s, T_p) combination that can cause the extreme event. Due to significant aerodynamic damping, the observed peak responses around the natural period are not observed during wind turbine operation.

Fig. 15 illustrates environmental inputs and the resulting responses, both in time and frequency domains. The dynamically amplified responses are caused by the wave loads, as validated by the signals' power spectral densities (PSD). For other support structures which are relatively not sensitive to waves, such as jacket foundations, this load case will not govern the design loads.

Based on a global sensitivity analysis of bottom-fixed OWT loads, hydrodynamic forces dominate the loads, particulary during parked or idling cases [45]. It is highlighted that the derived loads are based on linear irregular waves, which become invalid for steep waves. Nonlinear effects, such as springing and ringing-type responses, are not fully captured by the current load model. Wave models that incorporate full nonlinear effects and wave impact forces, as investigated by several researchers [46–51], provide more accurate load predictions. In cases where analytical and numerical calculations are subject to large uncertainties, validation against model tests to reduce the uncertainties, as demonstrated in several studies [19,52], are often recommended in design standards [24,30].

The derived annual maximum load distribution (see sec. 3.2.3) is illustrated in Fig. 16. A Gumbel distribution demonstrates a good fit to the 0.90 fractile levels, particularly at higher return periods ($CDF = 0.90,\ 0.98,\ 0.99,\ 0.998$). Note that extending the Gumbel fit to lower return periods ($CDF = 0.37,\ 0.80$) reduces the quality of fit at the higher return periods, which are more important to caputure when performing reliability analysis.

4.3. Example of reliability assessment

An example of reliability assessment based on the derived annual load distribution is demonstrated in this section. The preliminary support structure design is evaluated against bending failure due to extreme resonant response.

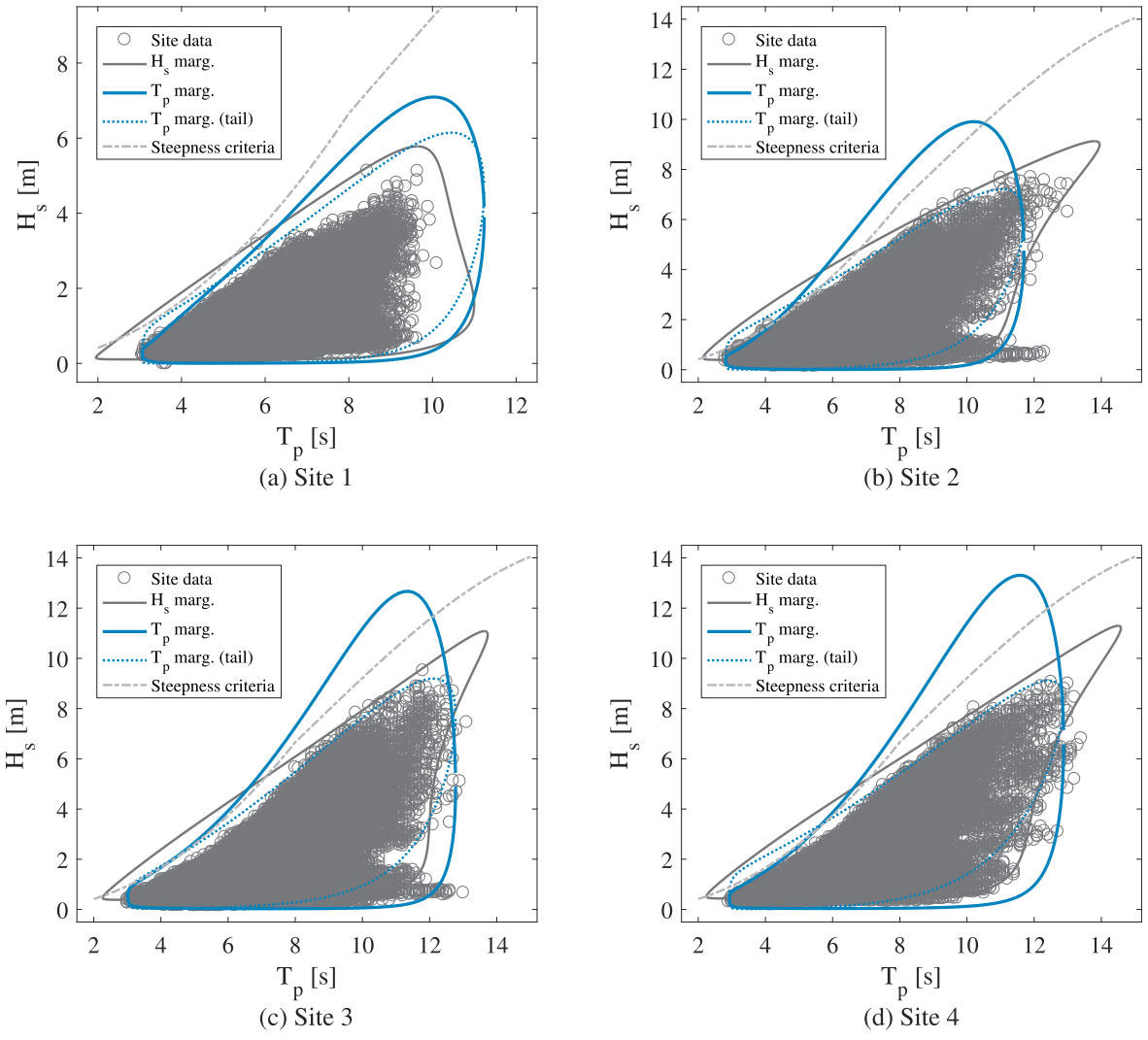

Fig. 13. Derived 50-year environmental contours at selected sites.

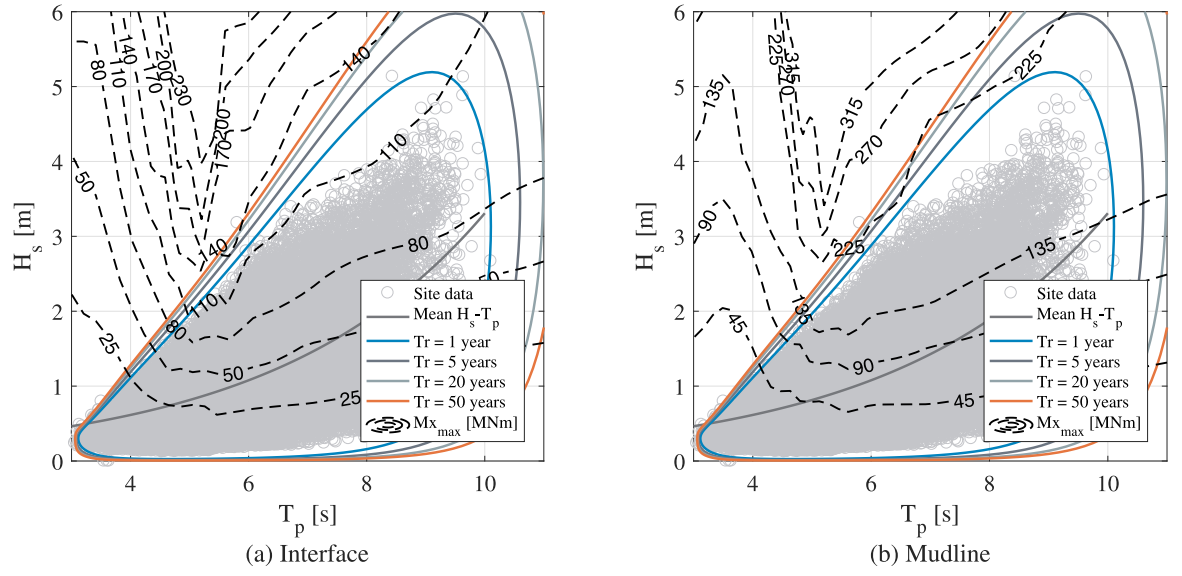

Fig. 14. Environmental contours plotted with monopile response isolines (Mx_{max} [MNm]).

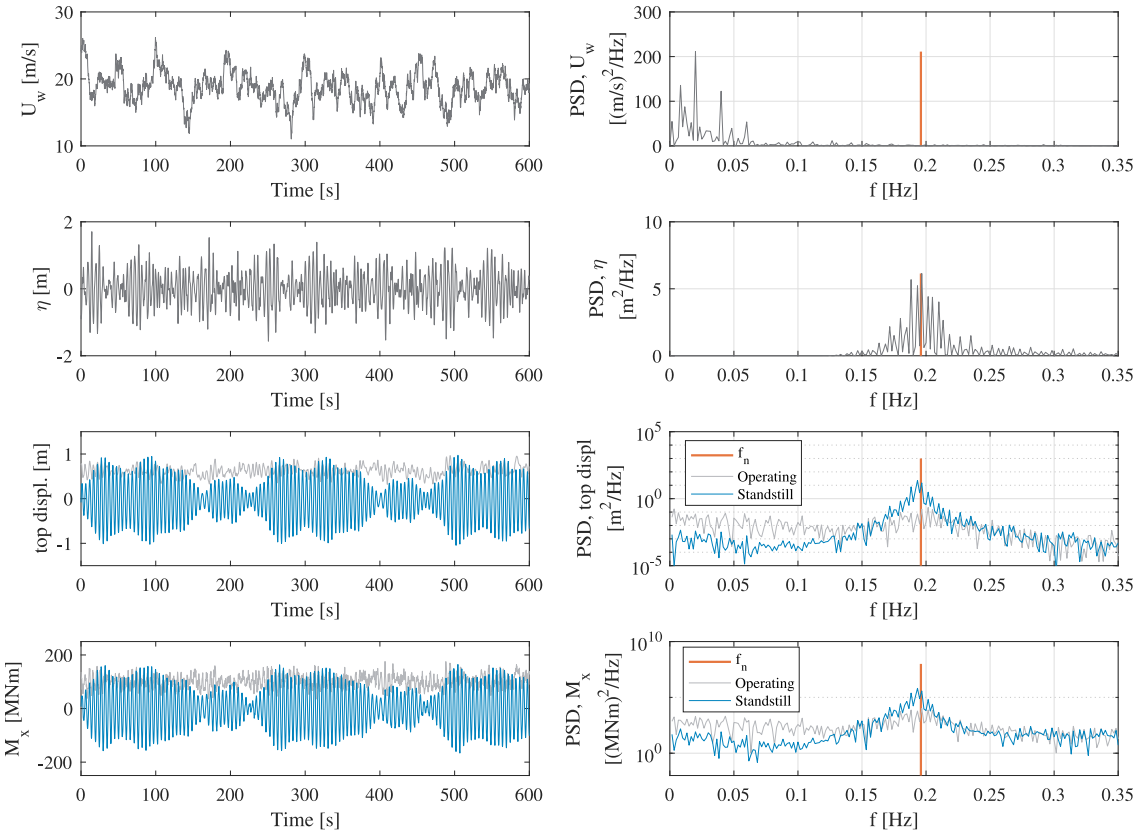

Fig. 15. Time and frequency domain signals of wind speed (U_w), wave elevation (η), and monopile responses for 1-year H_s return period (H_s = 2.05 m, T_p = 5.10, U_w = 18.7 m/s). The OWT natural frequency (f_n) is also plotted in the f-domain, with the PSD for monopile responses in log scale.

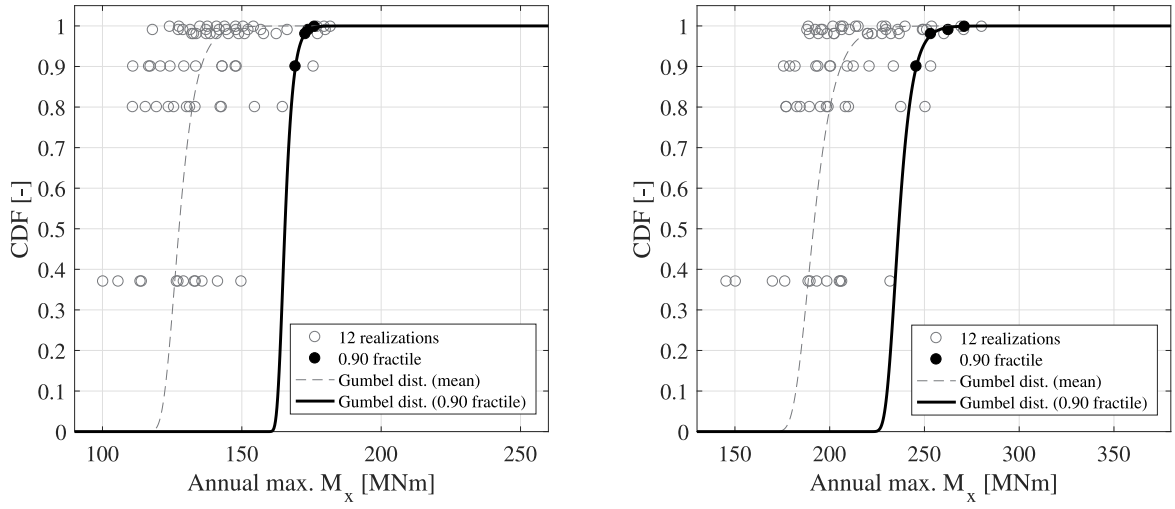

Fig. 16. Fitted Gumbel distribution to the annual maximum bending moment (M_x) at (a) interface (α_x = 164.7 *MNm*, β_x = 2.0 *MNm*, $E[M_x]$ = 165.9 *MNm* and σ = 2.6 *MNm*) and (b) mudline (α_x = 234.5 *MNm*, β_x = 5.0 *MNm*, $E[M_x]$ = 237.4 *MNm* and σ = 6.4 *MNm*) .

Table 6
Calculated annual reliability indices (β) for the monopile section at mudline.

t_{MP} [mm]	COV_{wave}				
	0.00	0.05	0.10	0.20	0.30
110	16.31	15.49	13.63	9.74	7.30
100	15.64	14.85	13.06	9.31	6.99
90	14.89	14.14	12.42	8.82	6.64
80	14.03	13.32	11.69	8.27	6.24

Table 7
Calculated annual reliability indices (β) for the tower section at interface .

t_{twr} [mm]	COV_{wave}				
	0.00	0.05	0.10	0.20	0.30
32	7.37	6.75	5.61	4.01	3.26
30	6.54	6.00	5.01	3.64	3.02
28	5.62	5.16	4.35	3.25	2.76
26	4.59	4.25	3.64	2.83	2.48

Table 8
Sensitivity factors (α_i^*) and design points x_i^* for COV_{wave} = 0.20, t_{MP} = 110 mm, and t_{twr} = 32 mm.

Stochastic variable, $\mathbf{x_i}$	Interface		Mudline	
	α_i^*	x_i^*	α_i^*	x_i^*
M_x	−0.070	166.0 MNm	−0.199	252.1 MNm
f_y	0.115	405.4 MPa	0.191	322.9 MPa
E_s	0.061	208.6 GPa	0.013	209.2 GPa
X_{wave}	−0.885	1.789	−0.860	4.951
X_R	0.440	0.856	0.428	0.663
X_{do}	0.034	0.999	0.041	0.998
X_t	0.016	1.000	0.011	1.000

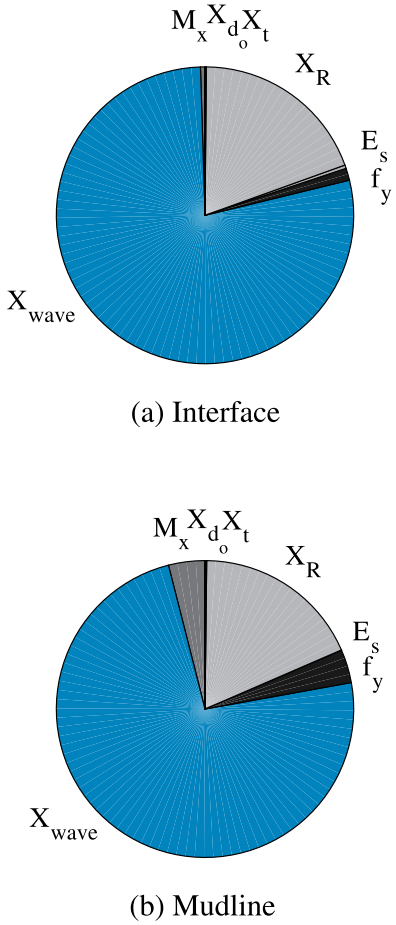

Fig. 17. Sensitivity (α_i^{*2}) of reliability index to stochastic input parameters for COV_{wave} = 0.20, t_{MP} = 110 mm, and t_{twr} = 32 mm.

Tables 6 and 7 summarize the calculated β for the monopile section at the mudline and tower section at the interface, respectively. The effect of section thickness (t_{MP}, t_{twr}) and wave load model uncertainties (COV_{wave}) to β is also shown. For all COV_{wave} and thickness range investigated, the mudline section have acceptable reliability levels. On the other hand, the interface level is more critical and can have unacceptable reliability levels ($\beta < 3.3$) for conditions with higher COV_{wave} and reduced t_{twr}. The same results were given by the deterministic design check (see sec. 3.2.3).

Along the *failure* surface, the sensitivity of $\beta(\mathbf{x})$ or $P_F(\mathbf{x})$ to the variation of stochastic parameter (x_i) is measured by the sensitivity factor (α_i) (see [27]). At the design points (x_i^*), the corresponding sensitivity factors (α_i^*) for COV_{wave} = 0.20 were determined, as summarized in Table 8. Since $\sum_i \alpha_i^2 = 1.0$, the sensitivity can also be illustrated as shown in Fig. 17. Results show that the $\beta(\mathbf{x})$ is most sensitive to uncertainties related to the wave load model (X_{wave}) and resistance model (X_R). On the other hand, variations in stochastic parameters E_s, X_{d_o} and X_t have relatively insignificant effects.

5. Conclusions and recommendations

In this paper, it was shown that extreme OWT loads can occur during parked or idling situations under operational wind speeds. A probabilistic assessment of offshore wind turbines under extreme resonant response was demonstrated. Based on in-situ wave observations on the North Sea, the environmental contour method is used to establish relevant design conditions. A case study on a large monopile foundation is presented to demonstrate that wave-sensitive, bottom-fixed foundations can have significant loads due to resonant behavior. Lastly, a simplified reliability analysis of both monopile and tower against bending failure is demonstrated. Although metocean characteristics and support structure designs are case-specific, the presented framework can be applied to assess the reliability of wave-sensitive OWT structures.

The accuracy of wave height extrapolations based on the EC method highly depends on the length and quality of data. Measurement and statistical errors, or model errors when using calibrated hindcast models, introduce uncertainties in establishing the design conditions. In addition, the traditional approach where H_s is modelled as the marginal distribution (with $Tp|H_s$), can overestimate H_s. When the interests are the non-extreme H_s, it is a good practice to compare metocean extrapolations with T_p or T_z as marginal distribution and H_s as the conditional parameter. Comparison with wave heights based on the steepness criteria [30] is also recommended.

The presented OWT responses are based on time-domain simulations with linear irregular waves. A more sophisticated wave model accounting for nonlinear effects, wave diffraction, and potential impact loads, is recommended for a more detailed assessment. Finally, it is highlighted that the reliability is generally more sensitive to load or response variations. Validation of numerical predictions based on model tests is very important for highly dynamic offshore structures.

As offshore wind turbines become bigger and as installations push to deeper waters, larger support structures become necessary. Upscaling of traditional bottom-fixed foundations can introduce design uncertainties, as these structures become more hydrodynamically sensitive. This study addresses design specifications, or the lack thereof, related to dynamic amplification due to wave-induced loads. Its implications on fatigue design will be further investigated.

Acknowledgements

This research work was performed within the European project INFRASTAR, which has received funding from the European Union's Horizon 2020 research and innovation programme under the Marie Skłodowska-Curie grant agreement No. 676139. All data used in this study were collected and made freely available by the EU Copernicus project and the programs that contribute to it. The authors are grateful to Prof. Ton Vrouwenvelder of TNO and Prof. Zhen Gao of NTNU for valuable discussions.

Appendix A. Derived parameters for environmental contours

Table A1
Parameters for the marginal and conditional distributions of the $H_s marg.$ model.

Parameters	Site 1	Site 2	Site 3	Site 4	Equation
α_1	1.436	1.192	1.225	1.273	Eq. (3)
β_1	0.951	1.016	1.318	1.450	Eq. (3)
γ_1	0.107	0.393	0.383	0.434	Eq. (3)
a_1	0.902	1.287	1.180	1.154	Eq. (5)
a_2	0.823	0.357	0.524	0.514	Eq. (5)
a_3	0.287	0.598	0.419	0.448	Eq. (5)
b_1	0.001	0.001	0.001	0.001	Eq. (6)
b_2	0.184	0.192	0.192	0.193	Eq. (6)
b_3	−0.251	−0.196	−0.196	−0.200	Eq. (6)

Table A2
Parameters for the marginal and conditional distributions of the $T_p marg.$ and $T_p marg.(tail)$ models.

Parameters	Site 1	Site 2	Site 3	Site 4	Equation
α_2	2.405	2.461	2.539	2.594	Eq. (8)
β_2	2.819	3.139	3.562	3.715	Eq. (8)
γ_2	3.050	2.799	2.998	2.899	Eq. (8)
m_1	0.000	0.000	0.000	0.000	Eq. (10)
m_2	0.031	0.062	0.097	0.058	Eq. (10)
m_3	2.059	1.828	1.623	1.919	Eq. (10)
n_1	2.586	2.233	−2.33E+01	−5.37E+01	Eq. (11)
n_2	5.45E+05	1.25E+02	3.05E+01	5.98E+01	Eq. (11)
n_3	−10.554	−3.296	−0.078	−0.027	Eq. (11)
p_1	0.000	0.000	0.000	0.000	Eq. (13)
p_2	0.023	0.064	0.060	0.071	Eq. (13)
p_3	2.229	1.869	1.931	1.876	Eq. (13)
q_1	0.000	0.000	0.000	0.000	Eq. 14
q_2	0.865	1.018	1.810	0.839	Eq. (14)
q_3	0.670	0.734	0.482	0.926	Eq. (14)

Appendix B. Illustrations of T_p marg. (tail) fitting method

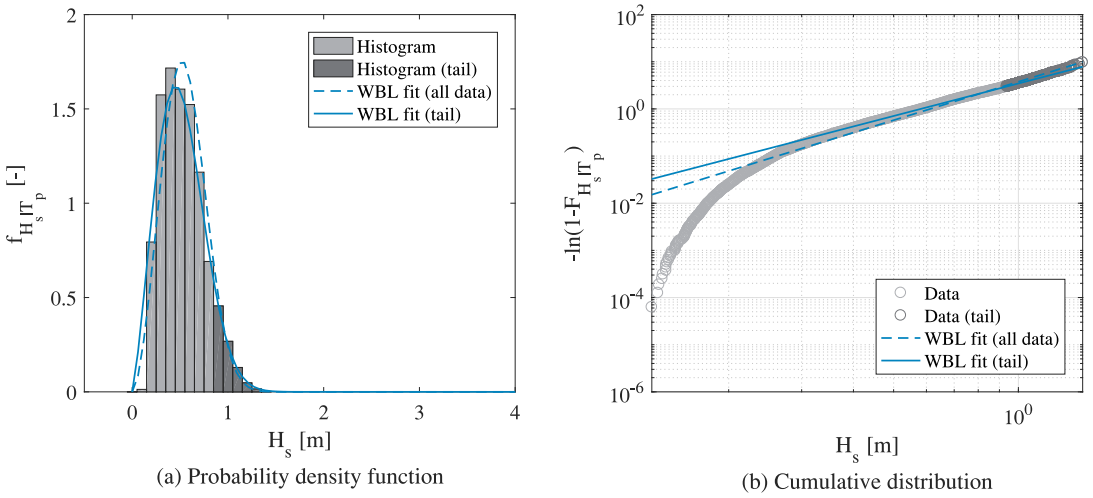

(a) Probability density function (b) Cumulative distribution

Fig. B1. Conditional wave height distribution fitted at 95th percentile of bin $T_p = [4.0 - 4.5]$: (a) probability density function $(f_{H_s|T_p}(h, t))$ and (b) cumulative distribution function $(F_{H_s|T_p}(h, t))$.

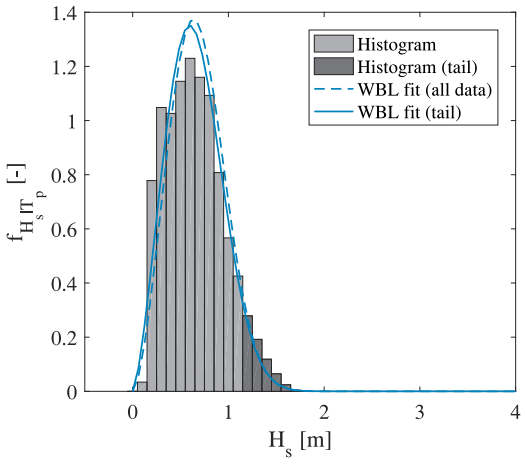

(a) Probability density function

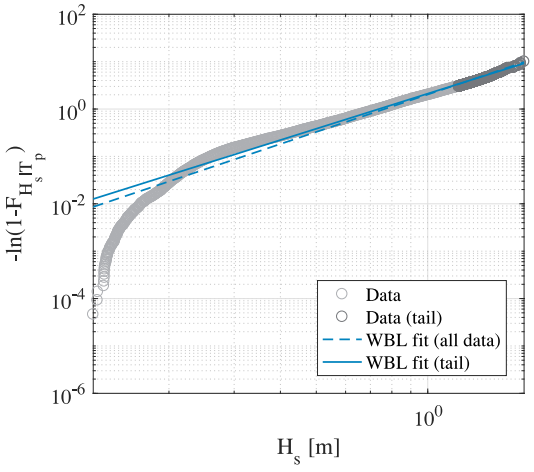

(b) Cumulative distribution

Fig. B2. Conditional wave height distribution fitted at 95th percentile of bin $T_p = [4.5 - 5.0]$: (a) probability density function ($f_{H_s|T_p}(h, t)$) and (b) cumulative distribution function ($F_{H_s|T_p}(h, t)$).

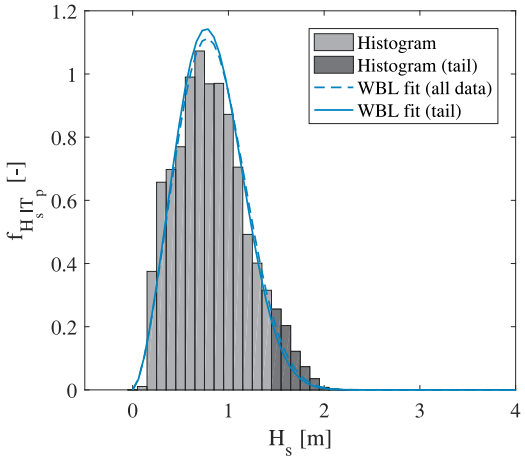

(a) Probability density function

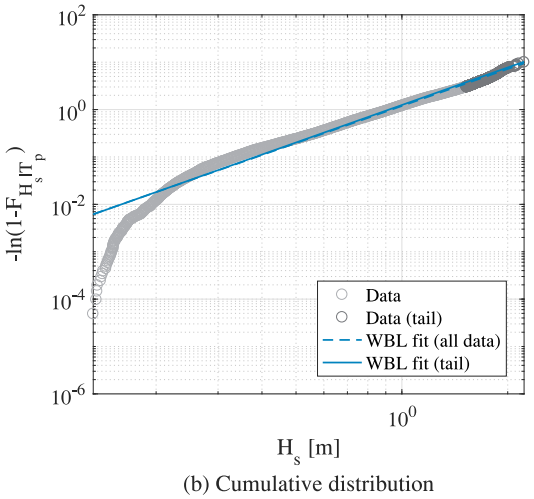

(b) Cumulative distribution

Fig. B3. Conditional wave height distribution fitted at 95th percentile of bin $T_p = [5.0 - 5.5]$: (a) probability density function ($f_{H_s|T_p}(h, t)$) and (b) cumulative distribution function ($F_{H_s|T_p}(h, t)$).

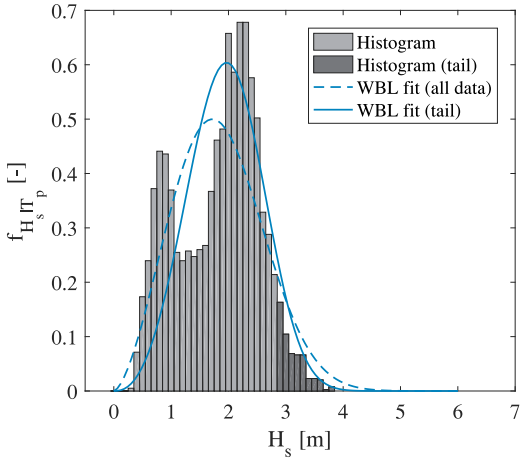

(a) Probability density function

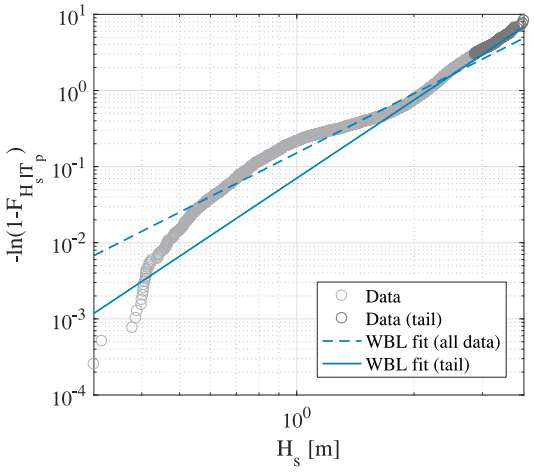

(b) Cumulative distribution

Fig. B4. Conditional wave height distribution fitted at 95th percentile of bin $T_p = [7.5 - 8.0]$: (a) probability density function ($f_{H_s|T_p}(h, t)$) and (b) cumulative distribution function ($F_{H_s|T_p}(h, t)$).

References

[1] S. Haver, Analysis of Uncertainties Related to the Stochastic Modelling of Ocean Waves, (1980).
[2] S. Haver, Wave climate off northern norway, Appl. Ocean Res. 7 (2) (1985) 85–92.
[3] S. Haver, On the joint distribution of heights and periods of sea waves, Ocean Eng. 14 (5) (1987) 359–376.
[4] E.M. Bitner-Gregersen, S. Haver, et al., Joint environmental model for reliability calculations, The First International Offshore and Polar Engineering Conference, International Society of Offshore and Polar Engineers, 1991.
[5] P. Jonathan, J. Flynn, K. Ewans, Joint modelling of wave spectral parameters for extreme sea states, Ocean Eng. 37 (11–12) (2010) 1070–1080.
[6] E.M. Bitner-Gregersen, Joint met-ocean description for design and operations of marine structures, Appl. Ocean Res. 51 (2015) 279–292.
[7] L. Li, Z. Gao, T. Moan, Joint distribution of environmental condition at five european offshore sites for design of combined wind and wave energy devices, J. Offshore Mech. Arct. Eng. 137 (3) (2015) 031901.
[8] E. Bitner-Gregersen, C. Guedes Soares, U. Machado, P. Cavaco, Comparison of different approaches to joint environmental modelling, 17th International Conference on Offshore Mechanics and Arctic Engineering, Lisbon, Portugal, Paper No. OMAE98-1495, (1998).
[9] L.V.S. Sagrilo, E.C.P. de Lima, A. Papaleo, A joint probability model for environmental parameters, J. Offshore Mech. Arct. Eng. 133 (3) (2011) 031605.
[10] E. Bitner-Gregersen, Joint long-term models of met-ocean parameters, in: C. Guedes Soares, Y. Garbatov, N. Fonseca, A. Teixeira (Eds.), Marine Technology and Engineering: CENTEC Anniversary Book, 1 2012, pp. 19–34.
[11] E. Vanem, Joint statistical models for significant wave height and wave period in a changing climate, Mar. struct. 49 (2016) 180–205.
[12] P. Jonathan, K. Ewans, Statistical modelling of extreme ocean environments for marine design: a review, Ocean Eng. 62 (2013) 91–109.
[13] S.R. Winterstein, T.C. Ude, C.A. Cornell, P. Bjerager, S. Haver, Environmental parameters for extreme response: Inverse form with omission factors, Proceedings of the ICOSSAR-93, Innsbruck, Austria, (1993), pp. 551–557.
[14] A.B. Huseby, E. Vanem, B. Natvig, A new approach to environmental contours for ocean engineering applications based on direct monte carlo simulations, Ocean Eng. 60 (2013) 124–135.
[15] A.B. Huseby, E. Vanem, B. Natvig, Alternative environmental contours for structural reliability analysis, Struct. Saf. 54 (2015) 32–45.
[16] C.F. Christensen, T. Arnbjerg-Nielsen, Return period for environmental loads–-combination of wind and wave loads for offshore wind turbines, EFP'99, (2000).
[17] K. Saranyasoontorn, L. Manuel, et al., On assessing the accuracy of offshore wind turbine reliability-based design loads from the environmental contour method, Int. J. Offshore Polar Eng. 15 (02) (2005).
[18] P. Agarwal, L. Manuel, Simulation of offshore wind turbine response for long-term extreme load prediction, Eng. Struct. 31 (10) (2009) 2236–2246.
[19] G.S. Baarholm, S. Haver, O.D. Økland, Combining contours of significant wave height and peak period with platform response distributions for predicting design response, Mar. struct. 23 (2) (2010) 147–163.
[20] Q. Li, Z. Gao, T. Moan, Modified environmental contour method for predicting long-term extreme responses of bottom-fixed offshore wind turbines, Mar. struct. 48 (2016) 15–32.
[21] E. Vanem, A comparison study on the estimation of extreme structural response from different environmental contour methods, Mar. struct. 56 (2017) 137–162.
[22] R. Shirzadeh, W. Weijtjens, P. Guillaume, C. Devriendt, The dynamics of an offshore wind turbine in parked conditions: a comparison between simulations and measurements, Wind Energy 18 (10) (2015) 1685–1702.
[23] S. Haver, G. Kleiven, Environmental contour lines for design purposes: why and when? ASME 2004 23rd International Conference on Offshore Mechanics and Arctic Engineering, American Society of Mechanical Engineers, 2004, pp. 337–345.
[24] NORSOK Standard, N-003-Actions and Action Effects, second ed., 1 Lysaker: Standards Norway, 2007.
[25] J. Velarde, J. Sørensen, C. Kramhøft, G. Zorzi, Fatigue reliability of large monopiles for offshore wind turbines, Int. J. Fatigue (2019). Submitted (under review)
[26] G. DNV, Loads and site conditions for wind turbines, Standard DNVGL-ST-0437 (2016).
[27] H.O. Madsen, S. Krenk, N.C. Lind, Methods of structural safety, Courier Corporation, 2006.
[28] M. Rosenblatt, Remarks on a multivariate transformation, Ann. Math. Stat. 23 (3) (1952) 470–472.
[29] ISOBSEN ISO, 19901-1: 2005, Petroleum and natural gas industries-specific requirements for offshore structures-part 1: metocean design and operating conditions, British Standards Institute (2005).
[30] DNV GL, Environmental conditions and environmental loads, Recommend Practice DNV-RP-C205 (2017).
[31] I.E. Commission, et al., IEC 61400-3, Wind Turbines–Part 3: Design Requirements for Offshore Wind Turbines (2009).
[32] E.M. Bitner-Gregersen, et al., Uncertainties in data for the offshore environment, Struct. Saf. 7 (1) (1990) 11–34.
[33] C. Bak, F. Zahle, R. Bitsche, T. Kim, A. Yde, L.C. Henriksen, A. Natarajan, M.H. Hansen, Description of the DTU 10 mw reference wind turbine, DTU Wind Energy Report-I-0092, 5 (2013).
[34] T.J. Larsen, A.M. Hansen, How 2 HAWC2, the user's manual, Technical Report, Risø National Laboratory, 2007.
[35] J. Velarde, E.E. Bachynski, Design and fatigue analysis of monopile foundations to support the DTU 10 mw offshore wind turbine, Energy Procedia 137 (2017) 3–13.
[36] W.N. WANDJI, A. Natarajan, N.K. Dimitrov, Influence of model parameters on the design of large diameter monopiles for multi-megawatt offshore wind turbines at 50-m water depths, Wind Energy (2017).
[37] L. Rayleigh, Theory of Sound, two volumes Dover Publications, New York, 1897.
[38] C. Devriendt, P.J. Jordaens, G. De Sitter, P. Guillaume, Damping estimation of an offshore wind turbine on a monopile foundation, IET Renewable Power Gener. 7 (4) (2013) 401–412.
[39] J. Mann, Wind field simulation, Probab. Eng. Mech. 13 (4) (1998) 269–282.
[40] H. Glauert, Airplane Propellers, Aerodynamic theory, Springer, 1935, pp. 169–360.
[41] M.O. Hansen, H.A. Madsen, Review paper on wind turbine aerodynamics, J. Fluids Eng. 133 (11) (2011) 114001.
[42] N. Standard, N-004-Design of Steel Structures, rev. 3, (2013). Lysaker: Standards Norway
[43] J. JCSS, Probabilistic model code, Joint Committee on Structural Safety (2001).
[44] I.S. Organization, ISO 2394: 2015: General principles on reliability for structures, 2015.
[45] J. Velarde, C. Kramhøft, J.D. Sørensen, Global sensitivity analysis of offshore wind turbine foundation fatigue loads, Renew Energy (2019), https://doi.org/10.1016/j.renene.2019.03.055.
[46] S. Schløer, H. Bredmose, H.B. Bingham, Irregular wave forces on monopile foundations. effect af full nonlinearity and bed slope, 30th International Conference on Ocean, Offshore and Arctic Engineering, American Society of Mechanical Engineers, 2011.
[47] P. Agarwal, L. Manuel, Incorporating irregular nonlinear waves in coupled simulation and reliability studies of offshore wind turbines, Appl. Ocean Res. 33 (3) (2011) 215–227.
[48] H. Bredmose, P. Slabiak, L. Sahlberg-Nielsen, F. Schlütter, Dynamic excitation of monopiles by steep and breaking waves: experimental and numerical study, ASME 2013 32nd International Conference on Ocean, Offshore and Arctic Engineering, American Society of Mechanical Engineers, 2013.
[49] S. Schløer, B.T. Paulsen, H. Bredmose, Application of cfd based wave loads in aeroelastic calculations, ASME 2014 33rd International Conference on Ocean, Offshore and Arctic Engineering, American Society of Mechanical Engineers, 2014.
[50] B.T. Paulsen, H. Bredmose, H.B. Bingham, An efficient domain decomposition strategy for wave loads on surface piercing circular cylinders, Coastal Eng. 86 (2014) 57–76.
[51] B.T. Paulsen, B. de Sonneville, M. van der Meulen, N.G. Jacobsen, Probability of wave slamming and the magnitude of slamming loads on offshore wind turbine foundations, Coastal Eng. 143 (2019) 76–95.
[52] E.E. Bachynski, T. Kristiansen, M. Thys, Experimental and numerical investigations of monopile ringing in irregular finite-depth water waves, Appl. Ocean Res. 68 (2017) 154–170.